FANC
federal agency for nuclear control

Appendix 1

1. What are the detection limits of the applied in-service inspections regarding hydrogen flakes?

The objective of the qualification of any Non-Destructive-Testing (NDT) procedure is to provide confidence that the procedure is fit for its purpose. In the present case, the purpose of the UT procedure using 0°L transducers is to detect and size a large population of quasi-laminar flaw indications having a maximum tilt angle of 15° (see Chapter 3 of the 2015 Safety Case). Of course, ensuring the detection of the whole population of the flakes is not feasible and therefore the objective of the qualification is to ensure that almost all the flakes are detected, while ensuring that all the significant flakes are detected.

The qualification of the UT inspection procedure by the Licensee aimed at ensuring the detection of a 6mm diameter flake having a tilt angle of 16° at a confidence level of 97.72%. The detection performance of a transducer depends, amongst other parameters, on the size, the tilt angle and the depth of the flake in the wall thickness. For any transducer, the objective of the UT inspection procedure is ensured for the most unfavourable combination of the tilt angle (16°) and depth (upper bound of the depth range of the transducer). That means that a 6mm flake having a tilt angle smaller than 16° and located at a depth lower than the upper bound of the transducer depth range is detected at a confidence level higher than 97.72%. Furthermore knowing that the tilt angle is a predominant parameter, this also means that flakes having a diameter less than 6mm but with a tilt angle smaller than 16°are also detected.

For flakes with a size smaller than the UT beam size, the reflector is punctual in front of the UT beam and the inclination is no longer a relevant parameter for the UT response. Therefore, the additional sensitivity needed to compensate for the inclination is no longer needed. This was shown through the extensive simulation work that was part of the qualification. UT indications smaller than the beam size will be systematically over-sized (to the beam size) by amplitude-based sizing techniques.

It is reminded that the UT reporting thresholds as defined by the qualification lead to report indications generating a UT response up to 2 exponent 5 times lower than the UT response obtained on the reference reflector, which is a side drilled hole of 2 mm diameter; this is representative of an extreme sensitivity level.

In addition to the demonstration of the detection performance of the UT procedure as achieved by the qualification, an illustration of the capability of the UT procedure to detect nearly the whole population of flakes is provided by the examination of the amplitude distribution curve of the indications (see paragraph 4.2.2 in the 2015 Safety Case[1]).

[1] In addition to the licensee reports, the same topics are also extensively addressed in the corresponding evaluation reports by the licensee nuclear safety department, and the Belgian Safety Authorities (FANC, Bel V and AIB-Vinçotte), published in January 2013, April 2013 and November 2015. For specific topics, additional reviews can be found in the Expert groups evaluation reports. All these reports are available on the FANC website.

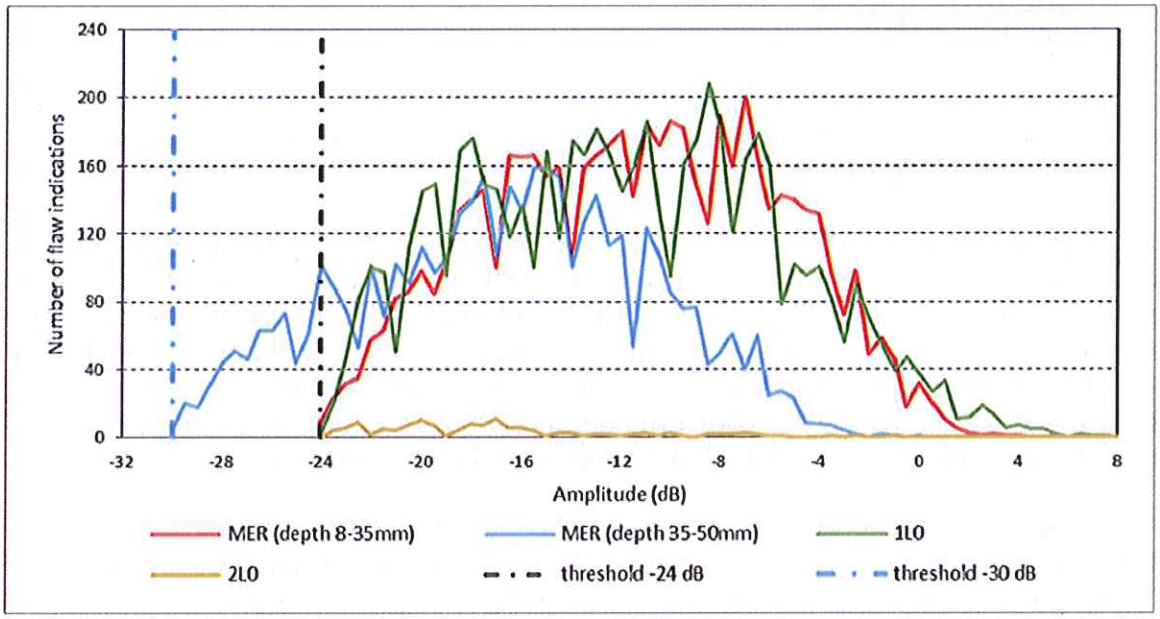

Figure 4.8: Indication amplitude distribution (4 shells).

Figure 1 – page 28 of the 2015 Doel 3 Safety Case

First, the "Gaussian" shape of the amplitude distribution curve for the different transducers conforms to the expectation for a large population of indications. Then and more importantly, for low values of the amplitude, the relationship between the number of indications and the amplitude (dB) is approximately linear. Finding that the left-hand side of the distribution curves is vanishing at the reporting threshold provides therefore additional confidence in the detection capability of the transducers.

2. **What are the criteria to distinguish between indications stemming from segregations and from hydrogen flakes?**

According to the Licensee experts and as confirmed by the AIB-Vinçotte experts, indications from segregation are not detected by the range of frequency generally used in the industry.

3. **How were shadowing and overlapping effects considered regarding the detectability and the sizing of defects?**

The concern expressed by this question was also raised by the Belgian Safety Authorities in 2013 and an action referred to as Action 5 was launched by the Licensee to provide the requested answer. That concern is addressed in the Addendum to the first Safety Case (see paragraph 2.2.2).

2.2.2 Partially Hidden Indications

Two samples with multiple hydrogen flakes were taken from block VB395/1 and examined. The dimensions resulting from their ultrasonic examination were compared to the results of their destructive examination. The comparison confirms the capability of straight beam ultrasonic testing (UT) to correctly detect and size hydrogen flakes that are partially hidden by others.

Requirement

In 'Doel 3 and Tihange 2 reactor pressure vessels – Provisional evaluation report (30 January 2013)', the FANC requires the following with regard to partially hidden flaws:

> *The licensee shall include a set of defects partially hidden by other defects for macrographical examination, to confirm whether the sizing method continues to function well.*

Steps taken: destructive examination of two samples

A first sample taken from block VB395/1 showed a partially hidden flake. This sample contains two partially overlapping indications: the lower one is partially hidden by the upper one. The destructive examination of this sample confirms the correct sizing of the flaws by straight beam UT inspection.

Also from block VB395/1, a second sample was extracted from a zone with a very high density of indications. A destructive examination was performed and reported. This sample contained four partially overlapping flakes, all correctly detected and sized by UT.

The destructive examination of both samples confirms that the straight beam UT examination applied during the 2012 in-service inspection ensures a good detection and sizing of indications. Moreover, the UT dimensions were oversized on both the X and Y axes.

Figure 2 – Page 14 of the addendum to the Doel 3 Safety Case - April 2013

Based on the results of the ultrasonic examination of block VB 395/1 that was used for the validation of the UT technique, two samples were taken from the block for destructive examination. The first sample contained two partially overlapping indications and the second one was taken from a zone showing a very high density of indications. The objective of the investigation was by comparing the size of the indications as obtained by the UT examination to the one measured by destructive examination, to demonstrate the capability of the UT technique to correctly detect and size hydrogen flakes partially hidden by others.

The destructive examination performed on the two samples confirmed that the 0°L UT technique enabled a good detection and sizing of the indications in the configurations examined, despite a very high density of indications contained in one of the samples.

4. **Was the dependence of the ultrasonic response on the tilt angle of the flaws considered only regarding the detectability of the flaws or was there also some adjustment of the sizing?**

The sizing capability of the UT examination using 0°L transducers was addressed by the Licensee and discussed with the Belgian Safety Authorities. This also included the potential dependency of the flaw sizing accuracy on the tilt angle.

This concern was first addressed by the validation of the UT technique performed during the 2012 Safety Case (see paragraph 4.3.4) using an UT Phased Array transducer including small-angle beams (-20° to +20°).

> **Assessing ultrasonic capability via destructive examination**
> The capability of the ultrasonic inspection was validated based on a destructive examination of 18 flaw indications of the specimen VB395/1. These indications were selected as representing a wide variety of flaws in terms of size, location and slope, or as relevant examples of neighbouring indications.
>
> Regarding the ultrasonic flaw detection capability, destructive testing did not show any material discontinuity that was not reported by the ultrasonic inspection.
>
> Comparison of the actual flaw dimensions and those measured by the ultrasonic straight beam test showed on average a slight oversizing, and no occurrence of significant undersizing. Such results are commonly seen as being of a high standard. It was also observed on three pairs of neighbouring indications that the ultrasonic evaluation of the sound material ligament between them is slightly underestimated, i.e. conservative.
>
> Finally, the ultrasonic measurements carried out with refracted and tilted beams spreading from -20° to 20° along two orthogonal axes concluded that, even on the most inclined hydrogen flakes, no flaw is missed and the flaw sizing quality is not degraded when only straight beam examination is implemented.

Figure 3 - Page 37 of the 2012 Doel 3 Safety Case – December 2012

A specific study of the higher tilted flaws was also performed (see paragraph 2.1.4 of the addendum to the 2012 Safety Case published in April 2013, pages 10 to 12).

The investigations allowed to conclude that, even on the most tilted hydrogen flakes from block VB 395/1, no flaw was missed and the flaw sizing quality was not degraded when only straight beam examination was implemented.

The accuracy of the sizing procedure was also investigated in the qualification of the UT inspection procedure using block VB 395/2. To this end, comparison was made for about one hundred flaw indications in block VB 395/2 between the size of the indications obtained by the UT examination to the one measured by destructive examination. From that it was

concluded that the sizing by the UT procedure was conservative but also that there was no correlation between the sizing error and the tilt angle.

5. How was the degree of the segregations in the forged RPV rings of Doel-3 and Tihange-2 estimated, i.e. their extent and the maximum concentrations?

The extent of the segregations in the forged RPV rings has been assessed by the Licensee based on the (macro-)segregation phenomenology in heavy shell forgings made from solid ingots, widely developed in the literature [1], [2], [3], [4]. Use has also been made of the outcomes of the "Heavy Forge Program" launched by AREVA in France around 1995. In particular, that research program allowed to predict the location and the shape of the macro-segregations in a forged shell based on the distribution of the segregations in the ingot and on the forging process. The theoretical extent of the macro-segregations – based on literature and models – has been verified for the specific case of the Doel 3 and Tihange 2 RPV forgings by performing a C-mapping and a macro-etching (natal) on both Doel 3 and Tihange 2 nozzle shell cut-outs (D3H1 and T2H2).
Moreover, knowing that the flakes are located in macro-segregations, the experimental evidence that the distribution of the flaw indications in the wall thickness of the affected ring forgings corresponds to the expected shape of the positive macro-segregations in the shells also contributes to the verification of the theoretical extent of the macro-segregations in the Doel 3 and Tihange 2 core shells.

The enrichment in impurities and alloying elements inside the macro-segregations has also been extensively investigated (see paragraph 3.1 in the 2015 Safety Case).

FANC

federal agency for nuclear control

3.1 Phenomenology of flaking

The concern was raised that the high number of flakes found in some areas of the RPV shells could be correlated with a high level of chemical enrichment inside the macro-segregation in those areas. A complementary evaluation of the level of segregation of the Doel 3 and Tihange 2 RPV forgings showed that no such correlation exists.

Context

The Safety Case Report and the Addendum confirm that the indications in the RPV shell can be associated with a zone of macro-segregations that is the result of complex mechanisms occurring during solidification of the ingot during fabrication. Moreover, the flaws are situated in very specific locations: the so-called 'ghost lines', which correspond to the residual features of the ingot after forging.
In addition, the Addendum explains why not all forged components of the Doel 3 and Tihange 2 RPVs contain the same amount of hydrogen flakes. Based on an analysis of the ingot size and the combined sulphur and hydrogen content, the forgings were ranked according to their susceptibility to hydrogen flaking. This revealed a good correlation with the amount of flakes found in each forged component.
During the discussion of the Safety Case Report, the concern was raised that the high density of flakes found in some macro-segregated areas of the RPV shells could be correlated with a high level of chemical enrichment inside those areas. If so, this would have to be considered when assuming initial fracture toughness values for those zones.

Approach

The level of segregation of the Doel 3 and Tihange 2 RPV forgings was evaluated through an empirical formula developed on the bases of examinations performed on a large number of conventional ingots. This formula gives the level of carbon enrichment in the final forging as a function of its average chemical composition. Since enrichment in other alloying elements is proportional to the carbon enrichment, the latter is thus a good indicator for the enrichment level of segregations. In order to validate the formula, the predicted enrichment for the nozzle shells of Doel 3 and Tihange 2 was compared to carbon enrichments levels measured on the respective D3H1 and T2H2 cut-outs from those shells. And for all forgings, the predicted segregation levels were compared to the observed numbers of hydrogen flakes.

Results

The predicted carbon enrichment levels for the Doel 3 and Tihange 2 RPV forgings are given in Table 3.1. The enrichment is expressed as the ratio between the difference between the maximum and minimum carbon content encountered in the final forging, and the average carbon content of the ladle.

RPV forging	Carbon enrichment [%]	Number of indications (2012)
Doel 3 Lower Core Shell	43.3	7205
Tihange 2 Upper Core Shell	49.2	1931
Tihange 2 Lower Core Shell	47.6	80
Doel3 Upper Core Shell	50.2	857
Doel 3 Nozzle Shell	45.6	11
Tihange 2 Nozzle Shell	50.8	0

Table 3.1: Comparison of carbon enrichment level and number of hydrogen flakes

The carbon enrichments measured on the Doel 3 and Tihange 2 nozzle cut-outs correspond well to the predicted values illustrating the applicability of the correlation to the Doel 3/Tihange 2 RPV forgings. As shown in Table 3.1, the forging with the highest number of flakes (Doel 3 Lower Core Shell) is the less segregated one, and the forging without any flake (Tihange 2 Nozzle Shell) is the most segregated one.

Conclusions

The evaluation shows there is no correlation between the number of hydrogen flakes encountered in the forging and the chemical enrichment of the macro-segregation that contains the flakes.

Figure 4 - Page 15 and 16 of the 2015 Doel 3 Safety Case - November 2015

The maximum C-enrichment in the macro-segregations of the different shells has been assessed by the Licensee using an empirical formula [5], based on the content of different alloying elements in the ladle and on the dimensions of the ingot. This allows to estimate the maximum segregation level, in the absence of experimental measurement. Indeed, the macro-segregation level of a zone is related to its C-enrichment (ΔC/C). The enrichment in all other alloying elements is proportional to the C-enrichment which is therefore a good indicator of the segregation [1].

The empirical formula [5] calculates the maximum C-enrichment in the macro-segregations as the value of ΔC/C where ΔC represents the difference between the maximum and the minimum C-content in the ingot after cropping and piercing and C is the carbon content of the ladle.
Applying the empirical formula [5] to the Doel 3/Tihange 2 RPV forgings yields the results shown in Table 1. Table 1 also includes for comparison the results obtained for a nozzle shell cut-out from a similar French plant (designated as H2BQ3). The calculation is based on the chemical composition of the ladle and on the dimensions of the ingots found in the construction file.

	ΔC/C [%]Calculated
D3 LCS	43,3
T2 UCS	49,2
T2 LCS	47,6
D3 UCS	50,2
D3 nozzle shell	45,6
T2 nozzle shell	50,8
H2BQ3	~48

Table 1: calculated C-enrichments

The size of these nozzle shell cut-outs is of the order of 1.2 m in diameter and 200 mm in thickness. In each component, a zone of macro-segregation was identified after cutting the component in two, polishing and etching of the sections (Figure 6, concerning D3H1).

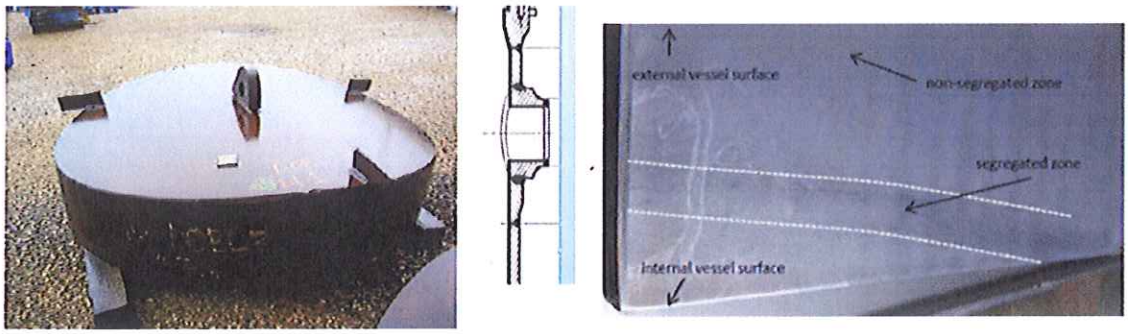

Figure 1: Doel 3 H1 nozzle cut-out and cross section after polishing and etching

Figure 5 – Doel 3 H1 nozzle cut-out and cross section after polishing and etching

C-mapping of three nozzle shell cut-outs allowed to determine experimentally the maximum C-enrichments. The measured maximum C-enrichments are 25 % for the D3 nozzle shell cut-out (D3H1), 30% for the T2 nozzle shell cut-out (T2H2) and 24% for the H2BQ3 nozzle shell cut-out.
The measured values of the maximum C-enrichment are not directly comparable to the calculated values. The measured maximum C-enrichment is indeed calculated as $(C_{max\ local} - C_{oS})/C_{oS}$ where $C_{max\ local}$ is the maximum local C-content in the macro-segregations and C_{oS} is the C-content out of the macro-segregations, both measured by C-mapping. However it is important to note that the ranking of the Doel 3 and Tihange 2 cut-out materials according to the maximum C-enrichment is predicted correctly by the empirical formula.

[1] C. Maidorn et D. Blind, «Solidification and segregation in heavy forging ingots,» Nuclear Engineering and Design, vol. 84, pp. 285-296, 1985

[2] D. Li, X.-Q. Chen, P. Fu, X. Ma, H. Liu, Y. Chen, Y. Luan et Y. Li, «How channel segregates originates: the flow of accumulated impurity clusters in solidifying steels,» Shenyang National Laboratory for Materials Science, Chinese Academy of Sciences, Shenyang

[3] G. Lesoult, «Macrosegregation in steel strands and ingots: characterisation, formation and consequences,» Materials Science and Engineering A, Vols. 1, 413-414, pp. 19-29, 2005

[4] D. Blind, W. Dietrich, W. Burr, K.-H. Katerbau et C. Maidorn, «Forschungsvorhaben Untersuchungen des Seigerungsverhaltens des Reaktorstahls 20MnMoNi55 an einem 180t-block,» MPA-Auftrags Nr.810044, Stuttgart, 1981

[5] J. Common, J. Delorme et P. Bastien, «Hétérogénéité des gros lingots de forge Etude de l'influence des impuretés et des éléments d'alliage sur la ségrégation,» Revue de Métallurgie, pp. 251-258, 1973

6. How was the influence of the segregations on the fracture toughness of the RPV materials assessed? How were the data from other known cases of pronounced segregations considered (KS02, top head and bottom of RPV for EPR projects)?

The effect of macro-segregations on the fracture toughness was already evaluated by the Licensee in the framework of the 2012 Safety Case (see paragraph 4.7.4 – pages 63 to 68) and is briefly summarized in the 2015 Safety Case (see paragraph 5.2.2 – pages 46 to 48). The Belgian Safety Authorities emphasized the importance of evaluating the impact of the macro-segregations on the fracture toughness for the two following reasons: (i) the demonstration of the flake stability is governed by the fracture toughness of the macro-segregated material where the flakes are located and (ii) the fracture toughness is expected to be lower in the macro-segregations due to the higher C-enrichment.

The effect of macro-segregations was investigated by the Licensee on three representative materials, i.e., the D3 nozzle shell cut-out (D3H1), the T2 nozzle shell cut-out (T2H2) and the H2BQ3 nozzle shell cut-out (see description above in the answer to question 5). Moreover, considering the C-enrichments predicted by the empiric formula (see Table 1 above), the material of the most affected ring shells (Doel 3 LCS and Tihange 2 UCS) have C-enrichments in their macro-segregations that are conservatively bounded by the C-enrichment of the D3H1 cut-out (lower bound) and the C-enrichment of the T2H2 cut-out (upper bound).

Fracture toughness tests on compact tension (CT12.5) specimens were performed in non-irradiated condition on specimens taken from the segregated and the non-segregated zones in the relevant orientation for laminar flaws (S-L) and in the "classical" (T-L) orientation.

For the D3H1 cut-out, tested independently by SCK•CEN and Areva (CT12.5 specimens), the difference in T_0 between the sampling position in the macro-segregation and out of it was less than 9°C in T-L orientation and 4°C in S-L orientation, which is not significant considering the standard deviation on T_0 (1σ = 4 to 7°C depending on the number of specimens). Note that for the tests in T-L orientation, the T_0 was lower in the macro-segregation than out of it. A detailed evaluation of the sampling position of the specimens in the macro-segregated zone shows that due to the small size of the zone with the highest degree of segregation, some specimens were taken in a zone with an intermediate degree of segregation. A detailed evaluation of the results for each specimen showed that there was no correlation between the fracture toughness and the degree of segregation. Alternative evaluations considering only the specimens with the highest $\Delta C/C$ ratio did not change significantly the T_0 value.

The H2BQ3 cut-out was tested in fracture toughness by Areva (CT12.5 specimens) and the two sampling positions (inside the macro-segregation and out of it) were only compared in the S-L orientation (orientation of the flakes). The same T_0 value was found for the two locations.

On the T2H2 cut-out, the fracture toughness was measured by Areva on CT12.5 specimens in S-L and T-L orientation. The difference in T_0 was 4°C in T-L orientation. The S-L orientation was only measured in the macro-segregation and the difference with the T-L orientation was only 4°C. In both cases these differences are not statistically significant.

In conclusion, the tests performed on three representative materials do not show any significant effect of the macro-segregation on the fracture toughness, as quantified by the difference in the Master Curve T_0 temperature.

If the T_{41J} temperature is used instead of the T_0 temperature, the difference in T_{41J} temperature between the macro-segregated zones and the non-segregated zones is insignificant for the D3H1 cut-out and 22°C for the T2H2 cut-out. Those values were used as the basis for defining the term $\Delta RT_{NDT,init\ (segregation)}$ in the predictive equation for irradiation embrittlement (see question 10).

The KS02 component is a RPV (half) flange rejected in the seventies due to the presence of a large number of indications, recently confirmed to be hydrogen flakes. This material was irradiated in the beginning of the eighties in the framework of a German research program (FKS program), focused at the time on the effect of macro-segregations. The KS02 component was forged from a solid 135 ton ingot (reduced by 49 ton after cropping top and bottom) into a 10.2 m long bar of rectangular cross section 0.77 x 1.43 m, shaped afterwards to form a half ring of external diameter 7.73 m. There was no piercing of the ingot and the whole segregation is kept inside the component, while most of it is removed by the piercing in the RPV shells.

No difference in irradiation sensitivity between the material taken in the macro-segregation or out of the macro-segregation was seen (see below) and the embrittlement is in line with the predictions of the modern trend curves, but there was a significant difference in Charpy properties (and to a lesser extent in fracture toughness) between the two zones in non-irradiated condition. The same difference remains after irradiation since the shift is similar for both materials.

In terms of Charpy properties, the difference between macro-segregated and non-segregated zones in KS02 is 31°C or 47°C at 41 J level on the energy curves, depending on the dataset (N° 31 or 32 respectively) used for the non-segregated material (Figure 7). For the lateral expansion data, the curve 31 is even closer to the "segregated" curve and the difference at the 0.89 mm level is only 6 J (less than the experimental uncertainty). The Shear Fracture Appearance data is not available for the "segregated" material so that no comparison is possible for this parameter.

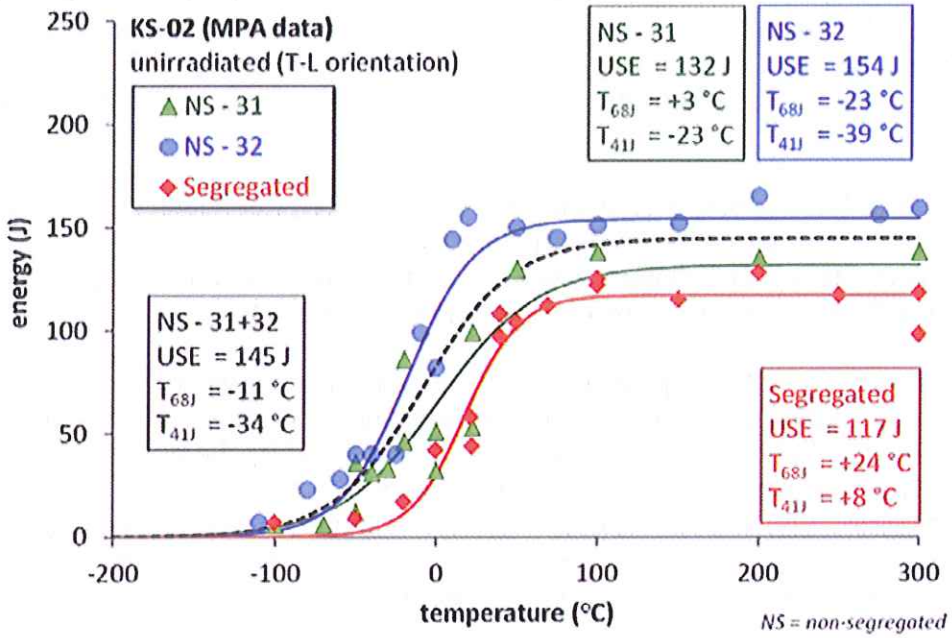

Figure 2: Charpy impact energy transition curves KS 02 B, non-segregated and macro-segregated areas

Figure 6 – Charpy impact energy transition curves KS02 B, non-segregated and macro-segregated areas

Fracture toughness data are also available and the maximum effect of the macro-segregation in the flake-affected materials is represented by the difference in To between macro-segregated and non-segregated zones and is 24.5°C (Figure 8). This difference is much smaller than the difference in Charpy curves.

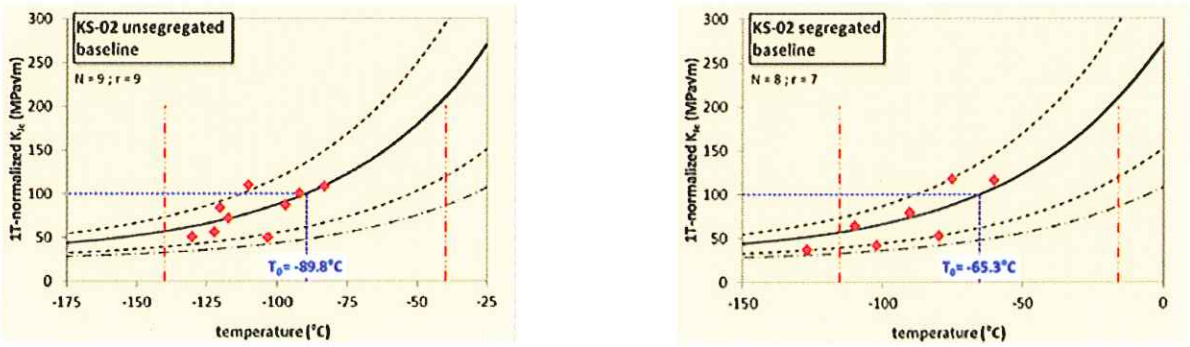

Figure 3. Fracture toughness KS 02 B, non-irradiated, non segregated and segregated

Figure 7 – Fracture toughness KS02B, non-irradiated, non segregated and segregated

In spite of the difference in Charpy curves, the NDT measured by Pellini drop weight tests is identical for the material in the macro-segregation and out of it (=0°C in both cases).

The RT_{NDT} determined according to ASME NB-2331 (or the German equivalent) is 0°C in the non-segregated zone and +3°C in the macro-segregated zone. For the non-segregated zone, the conditions on the Charpy energy and lateral expansion at T_{NDT}+33°C are fulfilled and RT_{NDT} = T_{NDT} = 0°C. For the macro-segregated zone, T_{68J}-33°C = 3°C is determining the RT_{NDT}.

This shows that there is only a very small difference in RT_{NDT} although the difference at the 41J level on the Charpy curves is much higher (31°C or 47°C depending on the selected non-segregated curve). This illustrates the fact that the difference in Charpy curves in non-irradiated condition is not a valid indication of the difference in RT_{NDT}.

The difference in T_{41J} between macro-segregated and non-segregated zones in KS02 is most likely due to the sampling location and to the mechanical properties gradient in a very thick forging (770 mm), the central part being much less affected by the quenching rate than the surfaces. The quenching rate effect is enhanced by the fact that only a relatively small segment (approx. 600 mm in length) from the component was quenched, not the full component. The Charpy specimens of the "non-segregated" material were sampled closer to the surface than ones from the "segregated" material.

Top and bottom heads of Flamanville RPV

According to the few publically available documents, the C-enrichment in the Reactor Vessel Head of the Flamanville EPR is significantly higher than the C-enrichment of the Doel 3 and Tihange 2 RPV core shell (about 50% for the EPR RPV top head). No information about the impact on the fracture toughness is available so far.

Irradiation effects on the macro-segregated zone

The irradiation effects on the macro-segregated zone are described in paragraph 5.2.3.2 of the 2015 Safety case for the D3H1 nozzle shell cut-out and in paragraph 5.2.3.3 for the KS02 flange.

In conclusion, no specific effect of irradiation on the facture toughness of the macro-segregation was identified in addition to the usual irradiation hardening effect.

7. What assumptions were made for the evaluations of the clad interface imperfections (defect location, orientation and size, fracture toughness)?

As discussed in paragraph 4.2.3 of the 2015 Safety Case, no specific assumptions were made for the evaluation of the clad interface imperfections. They were evaluated by the Licensee as hydrogen flakes.

4.2.3 Clad interface imperfections

As mentioned in the Doel 3 Safety Case report Addendum, the RPV UT inspections also revealed, in addition to the hydrogen flakes, indications located at the interface between cladding and base metal, that have been classified as clad interface imperfections (French: *défauts technologiques de revêtement* or DTR). In Doel 3, 268 such indications were found in the lower core shell and 33 in the upper core shell. The majority were thus located in the lower core shell, in the volume where the cloud of hydrogen flakes is situated close to the cladding-base metal interface.

Since for a number of those indications the distinction between DTR and hydrogen flake could not be made for 100% sure, it was decided to conservatively consider all of them as additional hydrogen flakes in the SIA.

A DTR is any flaw located at the cladding-base metal interface, that does not penetrate the base metal itself. A DTR should not be confused with underclad cracks (French: défauts sous revêtement or DSR), which are planar flaws at the cladding-base metal interface, located in the base metal, oriented perpendicular to the RPV surface and generated by cold cracking. No underclad cracks were discovered during the 2012 inspections.

Figure 8 - page 31 of the Doel 3 2015 Safety Case

8. **How was the possible impact of the different phosphorous concentrations on the degree of the segregations and their irradiation response considered, i.e. the content in the RPV rings of Doel-3 and Tihange-2 compared to the forgings VB395 and KS02?**

The effect of P-content on the segregation level is included in the empirical formula discussed above (see question 5).

The effect of P on the irradiation embrittlement is included in the RSE-M embrittlement trend curves considered in the Safety Cases. In the Safety Cases, the trend curves are built specifically for each core shell, taking into account the specific chemical composition of each core shell, and considering on top of that a lump-sum 14% enrichment of P in the segregated zone.

9. The conclusions from the evaluation of the integrity are based on calculations (linear-elastic fracture mechanics in combination with a modified characterisation of flaws according to ASME Code Case N-848). How was the applicability of the applied methods verified for the evaluation of inhomogeneous segregated zones in combination with the arrays of cracks actually present?

The main elements of this answer are presented in paragraph 5.4 'Large-Scale Validation Testing' in the Addenda 2013 of the Safety Case Reports (pages 37 to 40).

At the request of the Belgian Safety Authorities, structural tests on specimens containing hydrogen flakes [2][3] were performed by the Licensee with the following objectives:

- Demonstrating that the material has sufficient ductility and load bearing capacity, and that there is no premature brittle fracture.
- An experimental confirmation of the suitability and conservatism of the 3D extended finite elements analysis.

The tests were carried-out on several types of specimens:

- 4-points bending specimens on bars with hydrogen flakes
- tensile specimens containing hydrogen flakes or flawed with EDM notches.

All of these specimens were cut out of the AREVA shell VB395 containing flakes and segregated zones. The calculations (in linear elastic and in elastic-plastic conditions) were performed using the same methodology as in the Safety Cases as well as the same computational tools (extended finite element method).

One of the conclusions of those tests was that the failure loads of the specimens were always higher than those predicted before the tests, using the same methodology as for the Safety Case (flakes characterization and XFEM calculations).

This demonstrates the applicability and the conservatisms of the Fracture Mechanics calculations as performed in the frame of the Flaw Acceptability Analysis of Doel 3 and Tihange 2 RPVs [2][3].

[1] Doel 3 and Tihange 2 reactor pressure vessels: Provisional evaluation report ; FANC, 30/01/2013
[2] Safety case report – Addendum: Doel 3 – Reactor Pressure Vessel Assessment ; Electrabel, 26/04/2014
[3] Safety case report – Addendum: Tihange 2 – Reactor Pressure Vessel Assessment ; Electrabel, 15/04/2014

10. A transfer chain of terms was established for the determination of the reference temperature of the forged rings of Doel-3 and Tihange-2 after irradiation. This chain was based on the results from un-irradiated specimens of these rings (without segregation and without flakes) and from irradiated and un-irradiated specimens from VB395:
$RT_{NDT} = RT_{NDT,init} + \Delta RT_{NDT,init,segr} + \Delta RT_{NDT,RSE-M} + \Delta RT_{NDT,VB395} + M$

How was this chain of terms verified?

The different terms of the predictive equation for irradiation embrittlement are described in paragraph 5.5.2 of the 2015 Safety Case (page 68 to 72). That equation was the object of extensive discussions between the Belgian Safety Authorities and the Licensee, and its technical basis was validated by a panel of international experts (IRB – see IRB final report).

The first term ($RT_{NDT,Init}$) and the third term ($\Delta RT_{NDT,RSE-M}$) are the usual terms appearing in the 'standard' predictive equation for irradiation embrittlement and do not require any further comment.

The consideration of the second term ($\Delta RT_{NDT,Init,segr}$) was initiated from a recommendation of the IRB and was requested independently by the Belgian Safety Authorities. It is motivated by the concern that the initial RT_{NDT} of the macro-segregated zone could be higher than the one determined in the acceptance ring in the frame of the reception test.

The value of 10°C was determined mostly from the experimental results on the three nozzle cut-outs which were described in answer to question 6. It was recognized that components manufactured without piercing of the ingot (like KS02) are not representative of the RPV shells situation since the full macro-segregation is retained in the component while a large part is removed by the piercing in the RPV shells forged from solid ingots.

The fourth term ($\Delta RT_{NDT,VB395}$) was determined experimentally from the tests performed on irradiated specimens taken from the VB 395 shell and accounts for the specific irradiation embrittlement evidenced on that material (in the macro-segregated zones where flakes are located) in addition to the usual irradiation hardening embrittlement.

11. What are the load cases considered and how were the structural analyses performed in detail (loads during normal operation, transients and accidental loads, identification of the leading pressurized thermal shock (PTS) - transients, strip/plume cooling or axisymmetric thermal shock, linear-elastic or elastic-plastic material behaviour, consideration of residual stresses due to the cladding process, consideration of inhomogeneous material properties in the segregated areas, assumptions on defects)?

The main elements of the answer are presented by the Licensee in :

- paragraph 6.1.3 'Pressure and temperature loads' in the 2015 Safety Cases

6.1.3 Pressure and temperature loads

The transients from the Primary System design file were screened in order to determine the driving transients, i.e. the most penalizing transients with respect to brittle fracture, as a function of the position in the wall (ligament S), for the considered case of quasi-laminar flaws located in the core of the RPV shell. This screening identified the LOCAs (Loss Of Coolant Accidents) as being the driving transient for the first 20 mm from the cladding (inner side of the vessel wall), while the cool-down transients dominated in the next 10 mm and the heat-up transients in the deeper part of the wall (Figure 6.7).

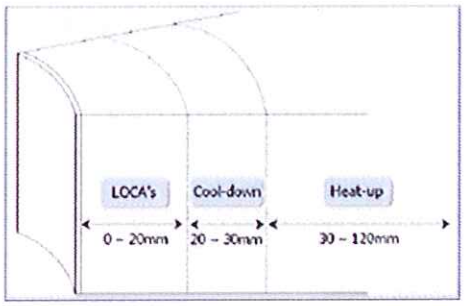

Figure 6.7: Determination of driving transients according to the ligament S.

Figure 9 - page 80 of the Doel 3 2015 Safety Case

- paragraph 4.1 'Effect of Ghost Lines on Mechanical Properties' in the Addenda 2013 to the first Safety Case Reports

4.1 Effect of Ghost Lines on Mechanical Properties

Tests performed on specimens from the Doel 3 H1 nozzle cut-out show that the ghost lines have no significant effect on the Charpy impact or fracture toughness properties.

Requirement

The following covers the mechanical testing part of this long-term requirement:

> *The licensee shall further investigate experimentally the local (micro-scale) material properties of specimens with macro-segregations, ghost lines and hydrogen flakes (for example local chemical composition). Depending on these results, the effect of composition on the local mechanical properties (i.e. fracture toughness) shall be quantified.*

Steps taken

To answer this requirement the following tests and analysis were performed on specimens taken from the Doel 3 H1 nozzle cut-out:

- **Charpy impact tests**

  Twelve Charpy impact specimens were taken with the notch at the level of a ghost line (crack propagation perpendicular to the plane of the ghost line). No difference is seen in the Charpy-impact test as compared to the curves established for the material free of ghost lines.

- **Fracture toughness tests**

  Eighteen fracture toughness tests were performed on pre-cracked Charpy specimens tested in three-point bending in the same orientation as the Charpys (sixteen tests in the transition and two in the ductile domain). The crack tip was positioned in the ghost line. Again, no significant difference is seen as compared to specimens without ghost lines. Scanning Electron Microscope analyses were performed on all fracture surfaces of the pre-cracked Charpy specimens. This confirmed the presence of zones of intergranular fracture at the crack front, which shows that the crack tip was well located within the ghost line. Other analyses, such as a chemical analysis, confirmed this finding.

- **Tensile tests**

  Three tensile tests were performed at 290 °C on specimens with a ghost line parallel to the specimen axis and on specimens with a ghost line perpendicular to the specimen axis.

  - For the tests with the ghost line perpendicular to the axis, the specimen broke outside of the ghost line. This is logical considering the higher yield stress of the ghost line.
  - For the specimens with the ghost line parallel to the specimen axis, the yield stress increases and the total elongation is reduced.

Conclusion

These analyses show that there is no significant effect of the ghost lines on the Charpy impact or fracture toughness properties.

Figure 10 - page 16 of the addendum to Doel 3 Safety Case - April 2013

- paragraph '4.2 Effect of Hydrogen Flakes on Material Properties' in the Addenda 2013 to the first Safety Case Reports (pages 22 to 25).

The considered load cases are the load cases of the design transient file of both units. All levels A, B, C and D transients of the design files were considered.

The identification of the governing transients was done through a screening of these transients with respect to the brittle fracture as a function of the position S in the wall thickness. This screening is summarized in the figure here below.

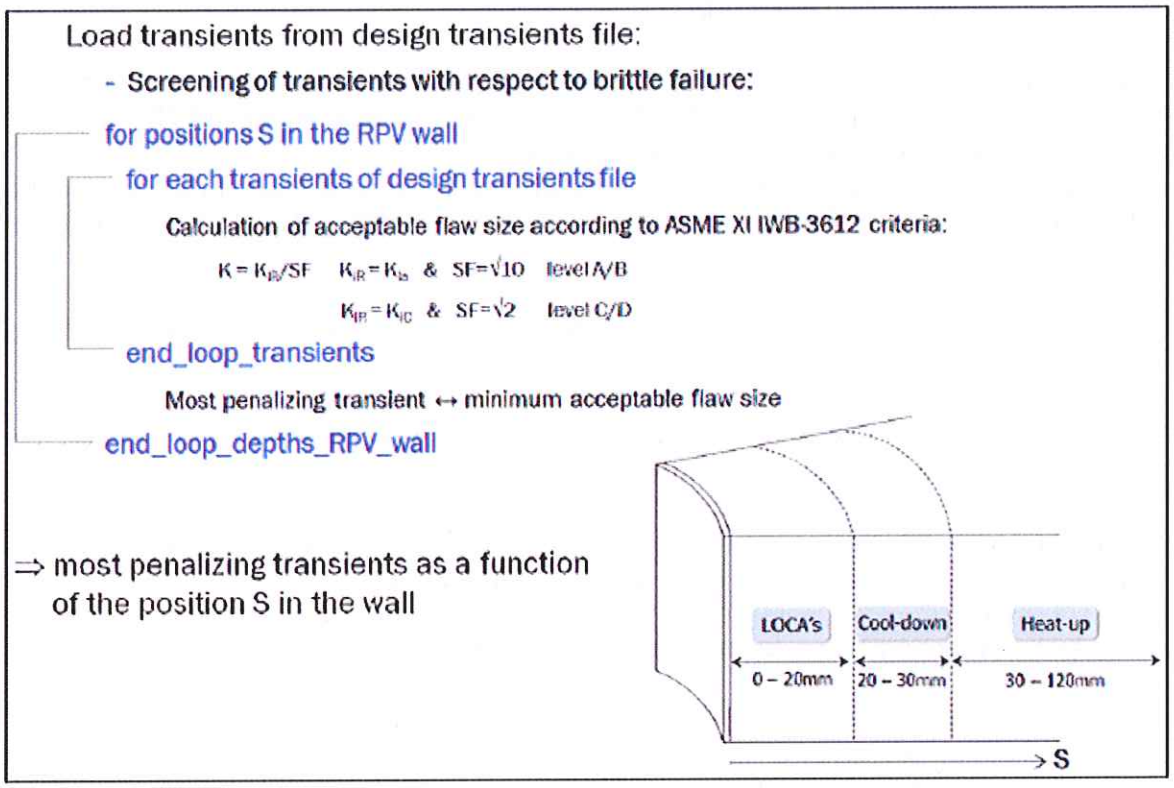

Figure 1 Screening of leading transients: principles and results
Figure 11 - Screening of leading transients : principles and results

This screening identified the Loss Of Coolant Accidents (LOCAs) as being the leading transient for the first 20 mm behind the cladding interface (inner side of the vessel wall), while the cool-down transients are leading in the next 10 mm and the heat-up transients in the deeper part of the wall.

The transient loadings issued from the design transient file are axisymmetric.

The Licensee argued that in the framework of protection against brittle failure, different computations performed for other RPVs have shown that the consideration of the plume effect (3D transient) leads to less severe safety margin than considering the axisymmetric design transient uniformly applied.
Indeed, the design transients are envelope transients (minimization of the temperature vs. time and maximization of the heat transfer coefficients vs. time).

These design transients are thus conservative in terms of thermal gradient, which leads to overestimate the thermal stresses in the vessel thickness in comparison to the actual 3D transients (i.e. accounting for plume effect).

On the basis of these design transients, the calculations of the crack driving forces and the assessment of the acceptable flaw size curves were done using:

- elastic-plastic behaviour of the material in the close-to-cladding area where LOCAs are leading transients, i.e. for $0 < S < 20mm$;
- linear elastic behaviour of the material in the area where cool-down and heat-up are leading transients, i.e. for $20mm < S$.

As far as the residual stresses induced by the cladding welding process are concerned, the RPV, before operating, has been subjected to a post-weld heat treatment (PWHT), which relieves most of the residual stresses in the cladding.
Moreover, after PWHT when RPV is cooled down, the residual stresses in the cladding are tensile in the cladding and slightly compressive in the base metal, close to the cladding-base metal interface area.

In addition, the RPV has been also subjected to two hydrotests at a pressure of $1.25 \times p_{design} = 215$ bars, which also tends to relief the residual stresses.

The residual stresses induced by the cladding process in the flaked area have been therefore considered by the Licensee as negligible.

Regarding the material properties in the macro-segregations, they were shown, through numerous experimental results, as not being significantly impacted by the inhomogeneous nature of the macro-segregations or by the presence of flakes. Therefore, the inhomogeneity of the material properties has been assumed by the Licensee as negligible for calculations.

Moreover, regarding the potential influence of the presence of the flakes on the thermal stress distribution, sensitivity analyses have demonstrated that the impact of hydrogen flakes on temperature distribution could be considered as low and the resultant effect on the flaw assessment was still lower.
That conclusion was achieved by the Licensee after having performed two bounding calculations at the request of the Belgian Safety Authorities. Both calculations consider a LOCA loading condition. In a first calculation, no heat transfer through the flakes is assumed by modelling the flakes with a small opening in the mesh. In the second calculation, perfect heat transfer through the flakes is assumed. When compared to the second calculation, the maximum stress intensity factor at the front of the flaws as obtained by the first calculation is slightly increased. As expected, that increase is due to the local increase of the thermal gradient at the crack front and between the flaws. The impact on the flaw assessment is however lower. Indeed, as the flaws act as thermal barriers, the temperature at the crack front is slightly increased and, as a result thereof, the material fracture toughness is slightly increased.

12. As the determination of the stress intensity at the hydrogen flakes under mixed mode loading (i.e. in modes I, II and III) an "equivalent stress intensity factor" was used. Was the applicability of this stress intensity factor validated for the loading situation (elastic-plastic with segregated areas) and the material state present in this case?

The definition and the use of the "equivalent stress intensity factor" were extensively discussed between the Belgian Safety Authorities and the Licensee. There were arguments based on theoretical considerations to support the definition of the equivalent stress intensity factor that has been used. Moreover, as explained in the answer to question 9, the validation of the equivalent stress intensity factor as well as the use of the J-integral was carried out through the numerous comparisons between the validation tests and their simulation, in linear elastic as well as in elastic-plastic conditions.

13. For the proof of the structural integrity of the RPV an elastic-plastic analysis of the load bearing capacity according to ASME BPVC Section III, Subsection NB-3228.3 was performed.

a. The method of ASME BPVC Section III, Subsection NB-3228.3 is normally applied to components free of flaws. How was the applicability of this method validated for RPV sections containing flaws?

The objective of the primary stress limits in NB-3000 of Section III of the ASME B&PV Code is to prevent the loss of load-carrying capacity of a vessel (which is referred to as collapse) with a design margin of 1.5. As any other reactor pressure vessel of Westinghouse design, the margin against collapse of the Doel 3 and Tihange 2 RPVs is not significantly higher than the specified design margin: the general primary membrane stress intensity Pm under the design pressure is lower by less than 5% than the design stress intensity value Sm. Otherwise stated, more than 95% of the RPV wall thickness is necessary to ensure the load-carrying capacity with the specified design margin. The RPV is therefore not tolerant to large radial flaws (radial flaws are critical in RPVs since they tend to be opened by the stresses due to internal pressure, and hence might grow with time). The hydrogen flakes encountered in the Doel 3/Tihange 2 RPVs have a much less critical orientation: they are quasi-laminar defects, meaning that they are almost parallel to the inner vessel wall surface. As such, they cannot be opened by the axial and circumferential stresses in the RPV wall. When applying the design-by-analysis rules of Section III, the material is assumed to be free of flaws.

Any reduction of the wall thickness due to the presence of flaw(s) lowers the load-carrying capacity of the vessel. For that reason, IWB-3610 (d) (2) in section XI of the ASME B&PV Code requires: The component containing the flaw is acceptable for continued service during the evaluated time period if [...] the primary stress limits of NB-3000, assuming a local area reduction of the pressure retaining membrane that is equal to the area of the detected flaw(s) as determined by the flaw characterization rules of IWA-3000, are satisfied.

The intent of that paragraph is to require that the presence of a flaw does not reduce the wall thickness to the extent that the load carrying capacity is lost, i.e., to the extent that the specified design margin against collapse is not satisfied.

Determining the reduction in thickness due to the presence of clustered flakes in conformity with the paragraph in Section XI does not appear an easy task if over-conservatism is to be avoided. For that reason, use has been made of the possibility given in Section III to use other methods than the elastic stress analysis to verify the objective of the primary stress limitation. The use of those alternative methods (limit analysis and plastic analysis) was accepted in Section III and therefore for the analysis of pressure vessels with sound material. However, there is technically no reason for not permitting their use for evaluating the collapse load of flawed components.

Finite element incremental elastic plastic analysis was performed on a 2D RPV model with flaws using plain strain assumption. The model may be seen as a cylindrical shell made from a uniform azimuthal distribution of identical sectors; the basic sector contains infinitely long cracks, the size and location of which represent the actual most adverse distribution of flakes in any cross section of any sector of the RPV. No formal validation of the method has been performed. However the results of the analysis have been reviewed to check whether no results non-conforming to the expectation were obtained and in particular whether the stress redistribution around the cracks was as expected. It was also verified that no local collapse occurred by reviewing the strain distribution in the vicinity of the cracks.

The results show that, although some part of the available margin is consumed by the presence of flakes, the specified design margin is still verified.

b. Which stress-strain curve of the material was used in the finite element analysis?

Since the ASME B&PV Code does not provide Stress-Strain curves, the σ-ε curves of the base metal have been obtained by shifting the typical RSE-M σ = f(ε) curves [1]. These tensile curves are made 'dimensionless' in [1] by the yield strength Sy.

For the ASME Section III calculation, the curve was multiplied by the yield strength at 345°C, Sy = 285.4 MPa, issued from the ASME B&PV Code Section II.

[1] RSE-M – Partie II: Annexes, Ed. 1997

c. What were the location(s) of the RPV where the stress-strain curve was determined and how were the strain concentrations considered at local discontinuities like hydrogen flakes?

The main elements of this answer are presented by the Licensee in paragraph 6.3 'ASME III – Primary Stress Reevaluation' of the 2015 Safety Case (page 89 to 91).

It follows from the answer to question 13b that the considered stress-strain curve is independent from the location in the RPV.

Several steps were followed by the Licensee to determine the flaw location of the RPV that was calculated with 2D finite elements:

- Highest density region

The first selection consists in retaining only the highest density region of the core shells. This rough selection is based on a density map and allows limiting the domain dimension for the next steps of the selection.

- Division in cells

In order to detect the local zones with highest density, the selected region is split into cells with $\Delta y=1.1° \cong 40mm$ and thin vertical slices of $\Delta x=0.5mm$.

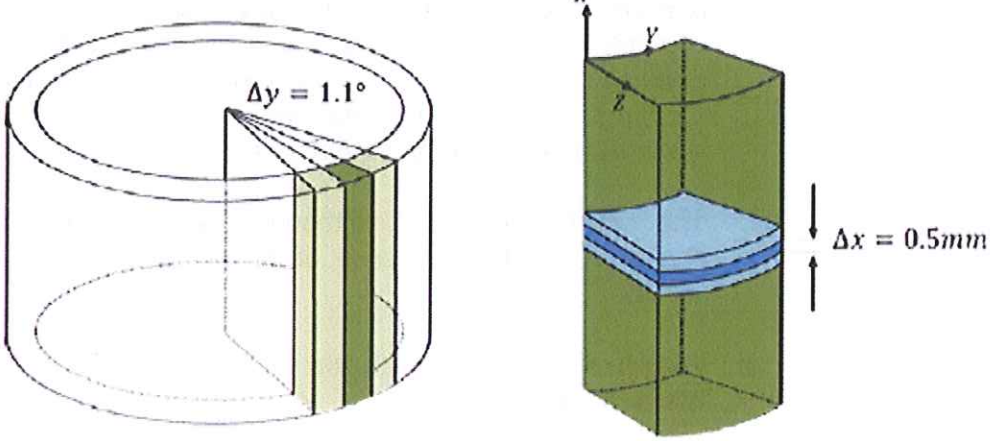

- Cell selection

In each of these cells, the number of flaws N_i included or even partially crossing cell i is calculated, as well as the sum of flaw projections on Z-axis.

The selected cell corresponds to the one having the highest number of flaws N_i, and with the highest sum of flaw projections on Z-axis.

- Flaw characteristics

The UT provides indications as boxes (white boxes below). The 2D flaw (red line below) is taken as the largest flaw with highest tilt included in the UT box.

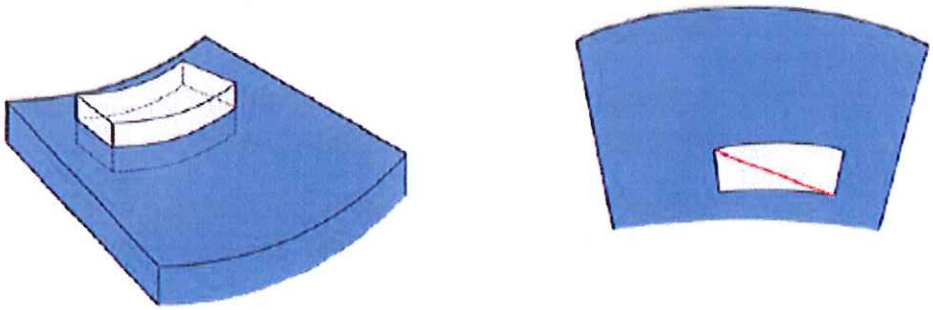

Following this methodology, the cells with the highest density include 8 flaws. Among these cells, the one with the largest sum of flaw projections on Z-axis of the RPV is selected.

Two calculations points were investigated:

- the point in the ligament between the two closest crack tips and
- the point in the most stressed area

Graphic representation of the flaws and calculation points are given in the figure below.

In doing so, the local discontinuities are accounted for in the calculations and the verification of the ASME Code Section III criterion

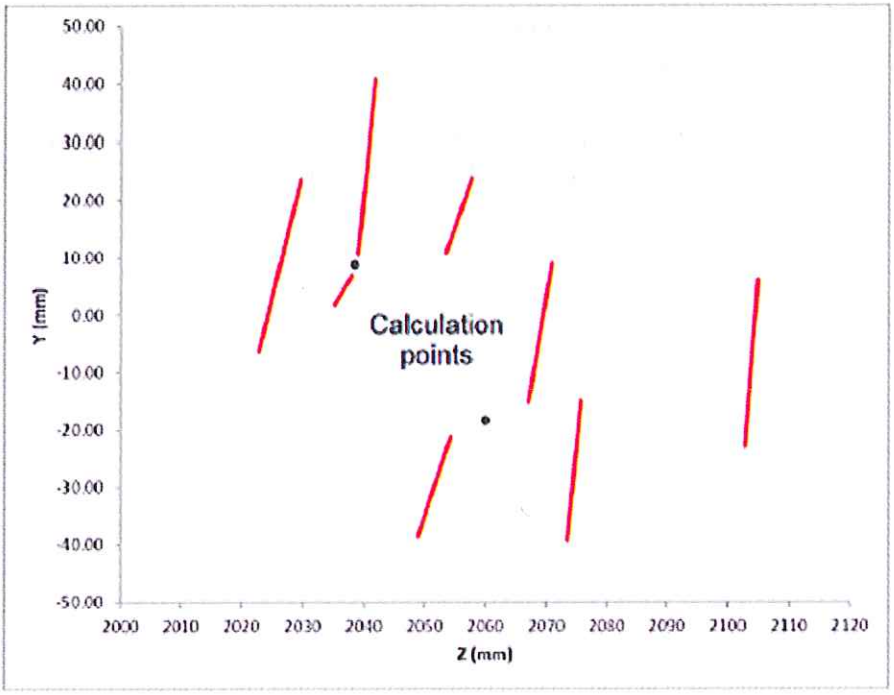

14. Was there any pressure testing of the RPV of Doel-3 and Tihange-2 after manufacture? If yes, at which pressure?

The main elements of this answer are presented in paragraph 6 'Load Tests' of the Addenda 2013 to the first Safety Case Reports (pages 42 to 45).

Hydrotesting of the RPV after manufacturing has been performed, as requested by the ASME Code Section III, at a pressure of 1.25 x design pressure, i.e. 215 bars.

That hydrostatic test pressure has been applied twice during the manufacturing and erection phases:

- the first for the RPV in the shop;
- the second for the primary system on site.

Since the start-up of the plants in 1982, no "hydrotest" has been performed except the load tests followed by UT re-inspection (p_{max} = 177 bars in Doel 3 and p_{max} = 178 bars in Tihange 2).

15. Is it (considered) necessary to perform structural analyses of postulated flaws in segregated areas (like the t/4 flaw according to ASME) in addition to the existing flaws?

The qualification process of the UT inspection procedure has demonstrated that the UT inspection procedure is capable of achieving at a high confidence level the detection of the flakes. It is therefore not necessary to consider in the Structural Integrity Assessment -any postulated flaw in addition to the ones detected by the UT inspection. .

The only flaw that has been postulated is the ¼ thickness flaw for the ASME Appendix G Analysis. For that analysis, account is taken of the material fracture toughness as obtained from the ASME XI fracture toughness curve indexed on the RT_{NDT} given by the predictive equation for the macro-segregated zones.